

Non-one-dimensional behavior in charge-ordered structurally quasi-one-dimensional Sr₆Co₅O₁₅A. S. Botana,^{1,2,*} P. M. Botta,³ C. de la Calle,⁴ A. Piñeiro,^{1,2} V. Pardo,^{1,2} D. Baldomir,^{1,2} and J. A. Alonso⁴¹*Departamento de Física Aplicada, Universidade de Santiago de Compostela, E-15782 Campus Sur s/n, Santiago de Compostela, Spain*²*Instituto de Investigacións Tecnolóxicas, Universidade de Santiago de Compostela, E-15782 Campus Sur s/n, Santiago de Compostela, Spain*³*Instituto de Investigaciones en Ciencia y Tecnología de Materiales (INTEMA), CONICET-UNMdP, J.B. Justo 4320 B7608FDQ, Mar del Plata, Argentina*⁴*Instituto de Ciencia de Materiales de Madrid (ICMM), CSIC, Cantoblanco, E-28049 Madrid, Spain*

(Received 17 September 2010; revised manuscript received 30 March 2011; published 19 May 2011)

We have synthesized Sr₆Co₅O₁₅, a quasi-one-dimensional oxide, measured its magnetic properties, and calculated its electronic structure by *ab initio* techniques. We have found strong evidence for its electronic and magnetic behavior not to follow the trend of its structural series. The magnetic coupling inside the CoO₃ chains is not purely ferromagnetic, and the long-range coupling inside the chains is very weak. The Co moments are slightly canted due to their large orbital angular momenta being oriented along each particular quantization axis, which is different for each Co⁴⁺ atom in the structure. Our thermopower calculations are in agreement with the experiment, supporting our model of the magnetic ground state of the compound.

DOI: 10.1103/PhysRevB.83.184420

PACS number(s): 71.20.-b, 75.25.Dk, 75.47.Lx

I. BACKGROUND

Transition-metal oxides have drawn the attention of the scientific community for the past 50 years. Particularly, cobalt oxides are becoming increasingly important because of their interesting properties such as superconductivity,¹ colossal magnetoresistance,² or phase separation.³

To elaborate models for strongly correlated electron materials, one-dimensional (1D) systems are key since they are the easiest to study because all the interesting phenomena take place along one direction. In this regard, there has been much interest in analyzing the homologous series $A_{n+2}B'B_nO_{3n+3}$ (Refs. 4–6) [A stands for alkaline or alkaline-earth cations, B' and B commonly correspond to Co cations in a trigonal prismatic and octahedral position, respectively, and $n \in [1, \infty)$], where the 1D chain is represented by $B'B_nO_{3n+3}$. Boulahya *et al.*⁷ reported the integer terms of the series which can be stabilized with Co occupying both octahedral and prismatic sites, by varying the nature and the proportion of alkaline-earth cations.

In particular, the two end members of the series [Ca₃Co₂O₆ ($n = 1$) and BaCoO₃ ($n = \infty$)] have been the focus of much attention over the past years. The $n = 1$ compound (Ca₃Co₂O₆) has been analyzed in several previous works.^{4,8–14} The valence state of Co ions in this case is assigned to be 3+, with a low spin state for Co ions in the CoO₆ octahedron ($S = 0$) and a high spin state within the trigonal prism ($S = 2$). This compound shows a paramagnetic behavior at high temperature. In-chain ferromagnetic (FM) interactions arise below 80 K, reaching 1D FM order at 30 K. Below this temperature, interchain two-dimensional (2D) antiferromagnetic (AFM) interactions appear, evolving into a ferrimagnetic order below 24 K (FM order within the chains that are partly antiferromagnetically coupled). According to Wu *et al.*,¹³ the FM intrachain interactions obey an Ising-type model due to the strong spin-orbit coupling effects on the Co ions within a trigonal prismatic environment. However, Cheng *et al.*¹⁴ affirm that the FM intrachain–AFM interchain competition invalidates the application of an Ising model. This material

has attracted much attention due to the magnetization plateaus observed in the magnetization versus field curves.⁸

The $n = \infty$ member (BaCoO₃) has also drawn considerable interest.^{4,15–23} It crystallizes in a 2H hexagonal pseudoperovskite structure, in which there are just face-sharing CoO₆ octahedra forming the 1D CoO₃ chain. In this case, the valence state of the Co atoms is 4+. *Ab initio* calculations predicted a FM ground state along the chains.¹⁸ The c axis is assigned to be an easy direction for the magnetization, leading to a large value of the orbital angular momentum. Also a large Ising-type magnetocrystalline anisotropy has been estimated.²²

The introduction of prisms in the structure of 2H-BaCoO₃ is accompanied by a decrease of the c_{2H} parameter. Keeping $B = \text{Co}$, to increase the P/O ratio ($P = \text{prism}$, $O = \text{octahedra}$), control of both temperature and annealing time as well as the adequate selection of an A cation is required to prepare these materials. The distance between A cations is one of the main factors governing the structural type which can be stabilized in the $A_{n+2}B'B_nO_{3n+3}$ series.

For this reason, there are fewer works on the magnetic or electronic structure properties for compounds with $2 \leq n \leq \infty$. The work by Sugiyama *et al.*⁴ studied the electronic structure and magnetic properties of the members $n = 1, 2, 3, 5$, and ∞ . The study reported an n -dependence of the charge and spin distribution of the Co chains. They proposed a charge distribution within the chains based on Co⁴⁺ cations (located in octahedra) and Co³⁺ ones (located in both trigonal prisms and octahedra). The existence of a magnetic transition was shown for all the compounds. Above the temperature attributed to this transition (T_C^{on}), a relatively strong 1D FM order appears. They suggested that, for compounds with $n = 1, 2, 3$, and 5 , T_C^{on} is induced by an interchain 2D AFM interaction. Another magnetic study reported by Sugiyama *et al.*²⁴ confirmed the role of this 2D AFM interaction in the series. The structural work carried out by Harrison *et al.*²⁵ for the Sr₆Co₅O₁₅ phase ($n = 4$) reported that this compound is a 2H-hexagonal perovskite-related oxide (isostructural with Ba₆Ni₅O₁₅) phase described by Campá *et al.*²⁶ Structure, magnetic properties, and electronic structure of single crystals

of the oxygen-deficient compound $\text{Sr}_6\text{Co}_5\text{O}_{14.7}$ have been studied by Sun *et al.*²⁷ They showed this compound to have unique polyhedral chains, consisting of a random composite of octahedra + trigonal prisms and octahedra + intermediate polyhedra. The magnetic properties of the compound can be understood according to that structural picture, where the Co^{4+} ions are located in the octahedra and the Co^{2+} ones are in either the trigonal prisms or the intermediate polyhedra. Whangbo *et al.*²⁸ proposed an interpretation of the electronic structure of $\text{Sr}_6\text{Co}_5\text{O}_{15}$ using a Hückel tight-binding calculation.²⁹ According to their model, the polyhedral chains are composed of Co^{4+} ions in octahedral sites and Co^{2+} ions in trigonal prismatic ones. The electrical resistivity and Seebeck coefficient dependence with temperature of $\text{Sr}_6\text{Co}_5\text{O}_{15}$ have been measured in some previous works,^{30,31} as well as for the closely related compound $(\text{Sr}_{0.75}\text{Ba}_{0.25})_6\text{Co}_5\text{O}_{15}$.³²

The purpose of this paper is to analyze the electronic structure and special magnetic properties of the $n = 4$ member of the series, $\text{Sr}_6\text{Co}_5\text{O}_{15}$. We have synthesized polycrystalline samples of the compound, characterized and analyzed its magnetic properties experimentally. Moreover, we have studied its electronic structure by *ab initio* methods, analyzing the plausible magnetic configurations and obtaining the magnetic ground state of the system. Also, we have calculated the thermopower using the standard Boltzmann transport theory based on the electronic structure obtained by first principles.

II. EXPERIMENTAL AND COMPUTATIONAL DETAILS

The $\text{SrCoO}_{3-\delta}$ “H” polymorph, which is $\text{Ba}_6\text{Ni}_5\text{O}_{15}$ -like, was obtained in polycrystalline form by a citrate technique. Stoichiometric amounts of analytical grade $\text{Sr}(\text{NO}_3)_2$ and $\text{Co}(\text{NO}_3)_2 \cdot 6\text{H}_2\text{O}$ were dissolved in citric acid. The solution was slowly evaporated, leading to an organic resin which was dried at 140°C and slowly decomposed at 600°C for 12 h. The sample was then heated at 900°C in air. The hexagonal phase was obtained by slowly cooling in the furnace. The reaction product was characterized by x-ray diffraction (XRD) for phase identification and to assess phase purity. The characterization was performed using a Bruker-axis D8 diffractometer (40 kV, 30 mA) in Bragg-Brentano reflection geometry with $\text{Cu } K\alpha$ radiation.

Neutron powder diffraction (NPD) patterns were collected at the Institut Laue-Langevin, Grenoble (France). The diffraction patterns were acquired at the high-resolution D2B diffractometer with $\lambda = 1.594 \text{ \AA}$, at 295 and 5 K in the angular range $10^\circ < 2\theta < 156^\circ$ with 0.05° steps. NPD diffraction patterns were analyzed by the Rietveld method,³³ using the FULLPROF refinement program.³⁴ A pseudo-Voigt function was chosen to generate the line shape of the diffraction peaks. The coherent scattering lengths for Sr, Co, and O were 7.020, 2.490, and 5.803 fm, respectively. The following parameters were refined in the final run: scale factor, background coefficients, zero-point error, pseudo-Voigt corrected for asymmetry parameters, positional coordinates, and isotropic thermal factors.

The magnetization (M) between 5 and 320 K was measured in a superconducting quantum interference device magnetometer (Quantum Design) under a dc magnetic field $H = 100 \text{ Oe}$. Data were taken upon heating in both zero-field-cooling (ZFC) and field-cooling (FC) regimes.

The electronic structure calculations were performed with the WIEN2K code,³⁵ based on density functional theory (DFT) utilizing the augmented plane-wave plus local orbitals method (APW + lo). For the calculations of the transport properties we used the BOLTZTRAP code,³⁶ that takes the energy bands obtained using the WIEN2K software.

For this moderately correlated transition-metal oxide, we used the LDA + U (Ref. 37) approach including self-interaction corrections in the so-called “fully localized limit” with an on-site Coulomb repulsion $U = 4.8 \text{ eV}$ and an on-site Hund’s rule coupling $J = 0.7 \text{ eV}$. This method has proven reliable for transition-metal oxides, since it improves over the generalized gradient approximation (GGA) or local density approximation (LDA) in the study of systems containing correlated electrons by introducing the on-site Coulomb repulsion U . Results presented here are consistent for values of U in the interval from 4 to 8 eV, in a reasonable range compared to other similar cobaltates,^{13,22} to describe correctly the semiconducting behavior of the material and the localized nature of the Co $3d$ electrons.

The calculations were fully converged with respect to the k mesh and $R_{\text{mt}}K_{\text{max}}$. Values used for the k mesh were $6 \times 6 \times 6$ sampling of the full Brillouin zone for electronic structure calculations, and $21 \times 21 \times 21$ for the transport properties. $R_{\text{mt}}K_{\text{max}} = 6.0$ was chosen for all the calculations. Selected muffin tin radii were as follows: 1.82 a.u. for Co, 2.28 a.u. for Sr, and 1.61 a.u. for O. Based on scalar relativistic basis functions, spin-orbit coupling (SOC) effects were included in a second-variational procedure.³⁸

III. RESULTS

A. Structure

The crystal structure (see Table I) of this phase was refined by a Rietveld analysis of the NPD data and published by some of us³⁹ in the $R32$ space group (No. 155), $Z = 3$, at room temperature and at 5 K, starting from the model defined by Harrison *et al.*²⁵ It contains two strontium, three cobalt, and three oxygen atoms in the asymmetric unit. The refinement of the occupancy factor for the Co atoms leads to a significant

TABLE I. Atomic positional parameters and occupancies for the $\text{Sr}_6\text{Co}_5\text{O}_{15}$ “H” phase after Rietveld refinement of NPD data at 5 K. The space group of our compound is $R32$ (No. 155). The lattice parameters are $a = b = 9.4740(1) \text{ \AA}$, $c = 12.360(1) \text{ \AA}$, and $V = 960.8(1) \text{ \AA}^3$. The reliability factors are $\chi^2 = 1.70$, $R_p = 4.67\%$, $R_{\text{wp}} = 6.33\%$, and $R_{\text{Bragg}} = 7.9\%$.

Atom	Cryst. pos.	Cryst.			Occup.
		x	y	z	
Sr1	9e	0.6437(5)	0	0.5	0.5
Sr2	9d	0.3210(5)	0	0	0.5
Co1	3b	0	0	0.5	0.114(7)
Co2	6c	0	0	0.103(1)	0.3333
Co3	6c	0	0	0.296(1)	0.3333
O1	9d	0.8436(9)	0	0	1
O2	18f	0.4946(7)	0.6728(7)	0.4785(3)	0.48(2)
O3	18f	0.8436(5)	-0.0240(5)	0.6088(3)	1

reduction (6%) of its contents for Co1, whereas Co2 and Co3 remained stoichiometric. The oxygen occupancy was slightly deficient for O2 and fully stoichiometric for O1 and O3. The refined crystallographic formula was $\text{SrCo}_{0.78(1)}\text{O}_{2.48(2)}$. According to this formula, the average oxidation state for Co is $3.79(1)^+$. The presence of Co_3O_4 , segregated from the main phase during the synthesis process, was quantified as 2%.

Both Sr atoms are eightfold coordinated by O atoms [$\langle \text{Sr1-O} \rangle = 2.592(2) \text{ \AA}$, $\langle \text{Sr2-O} \rangle = 2.751(2) \text{ \AA}$] in irregular coordination. The atoms Sr1 and Sr2 are disposed in columns parallel to the c direction. Two cobalt atoms, Co2 and Co3 (site 6c) are octahedrally coordinated by oxygen atoms [$\langle \text{Co2-O} \rangle = 1.896(6) \text{ \AA}$, $\langle \text{Co3-O} \rangle = 1.905(6) \text{ \AA}$] and the third, Co1 (site 3b) occupies a distorted trigonal prism [$\langle \text{Co1-O} \rangle = 1.922(2) \text{ \AA}$ and $\text{O-Co1-O} = 76.8(4)^\circ$]. The crystal structure consists of isolated, infinite chains of face-sharing CoO_6 polyhedra running along the c direction, forming a trigonal lattice in the ab plane as can be seen in Fig. 1(b). The repeat unit for Co-O species consists of four distorted octahedra sharing faces intermingled with prismatically coordinated Co1 atoms [see Figs. 1(a) and 1(c)]. The interoctahedral cobalt-cobalt distances are $\text{Co2-Co3} = 2.39(3) \text{ \AA}$, $\text{Co2-Co2} = 2.54(3) \text{ \AA}$. The face-sharing prismatic-octahedra Co1-Co3 distance is $2.53(2) \text{ \AA}$. These results³⁹ are comparable with those obtained by Harrison *et al.*²⁵ for the $\text{Sr}_6\text{Co}_5\text{O}_{15}$ phase, although in our case we are in the presence of a more severely Co-deficient compound, with a slightly smaller cell volume of 968.3 \AA^3 at room temperature [969.6 \AA^3 for $\text{Sr}_6\text{Co}_5\text{O}_{15}$ (Ref. 25)] as corresponding to a higher average oxidation state for Co cations. The in-plane distance between Co chains is $\sim 5.62 \text{ \AA}$ in the “ideal” structure and is flanked, in the refined structure, by 5.54 and 5.75 \AA (measured between different pairs of Co atoms belonging to two neighboring chains).

B. An ionic model

Since the compound is a correlated semiconducting oxide,³⁰ an image based on an ionic point charge model (PCM) can give us a crude estimate of the possible electronic configuration of the material. We will use such a model to describe the charge distribution of the cations along the Co chain. We will consider possible ionic configurations for the different Co ions along the chain and calculate their total energy, just based on the electrostatic repulsion, simplifying to take into account only the first neighbor contribution, and neglecting other energetic terms.

Taking the usual valencies for Sr and O, the average valence for Co in the ideal stoichiometric compound $\text{Sr}_6\text{Co}_5\text{O}_{15}$ is $+3.6$. Following the PCM we have just described, the valencies of the Co ions can be distributed in two isoenergetic ways in order to minimize the Coulomb repulsion: (i) $4 \text{ Co}^{4+}(d^5) + 1 \text{ Co}^{2+}(d^7)$ and (ii) $3 \text{ Co}^{4+}(d^5) + 2 \text{ Co}^{3+}(d^6)$. Various ionic arrangements have been considered in the literature. According to the structure determined by Harrison *et al.*,²⁵ Sun *et al.*²⁷ proposed that $4 \text{ Co}^{4+} + 1 \text{ Co}^{2+}$ is the most suitable model because the polyhedral chain with four octahedral sites and one trigonal prismatic allows Co^{4+} and Co^{2+} to be located in different sites. Whangbo *et al.*²⁸ also suggested the $4 \text{ Co}^{4+}(d^5) + 1 \text{ Co}^{2+}(d^7)$ model using a Hückel tight-binding calculation. This would be what we called solution (i). Instead,

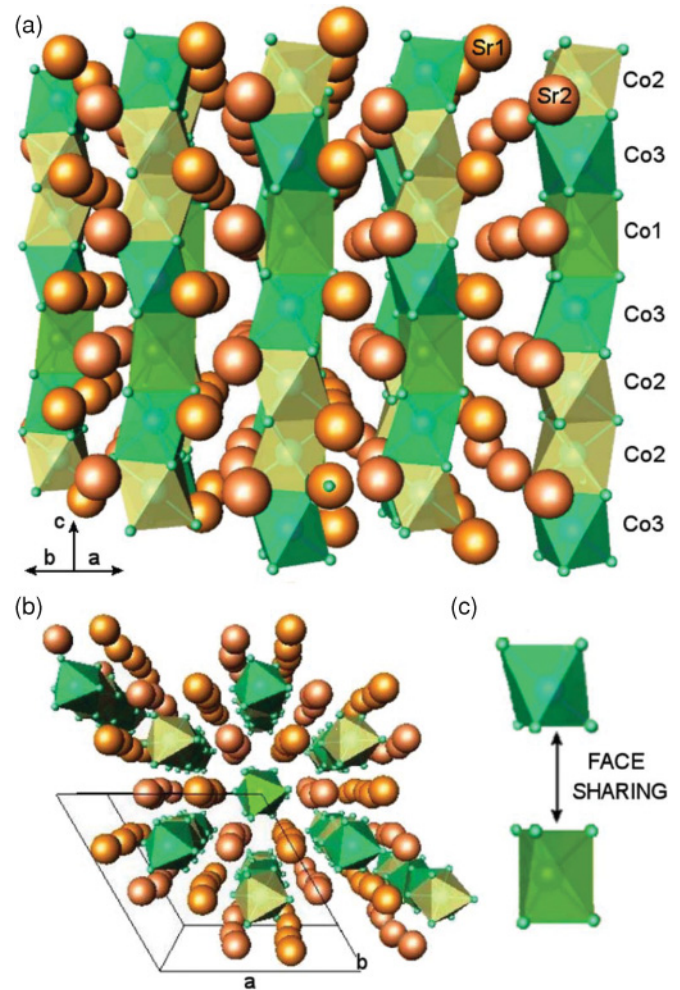


FIG. 1. (Color online) (a) Schematic picture of the structure of the CoO_3 chains in $\text{Sr}_6\text{Co}_5\text{O}_{15}$ showing the polyhedral environment of the different Co cations that occur along them. In the unit cell, formed by five Co atoms, four of them are situated in a distorted octahedron (green color) and one is in a trigonal prismatic environment (yellow color). (b) Top view of the structure of $\text{Sr}_6\text{Co}_5\text{O}_{15}$ showing the hexagonal symmetry of the ab plane, and the sixfold coordination of the Co atoms by O atoms. The in-plane distance between Co chains is significantly larger than the Co-Co in-chain distance, leading to the structural quasi-one-dimensionality. (c) Detail of the face-sharing arrangement along the chains.

Sugiyama *et al.*⁴ proposed the existence of at least one nonmagnetic atom in the chain for all the members of the series $A_{n+2}\text{Co}_{n+1}\text{O}_{3n+3}$: as n increases from 1 up to infinity, the Co valence increases from $+3$ and approaches $+4$ (e.g., for $n = 1$, the charge distribution in the unit cell is 2 Co^{3+} ; for $n = 2$, $2 \text{ Co}^{3+} + 1 \text{ Co}^{4+}$ and in our case for $n = 4$, $2 \text{ Co}^{3+} + 3 \text{ Co}^{4+}$). This we called solution (ii). In addition, in Ref. 4 it is suggested that the spin distribution for the two Co^{3+} ions in the chain is a high spin state (HSS) with $S = 2$ for the Co within a trigonal prismatic environment and a low spin state (LSS) with $S = 0$ for the octahedral one. Meanwhile, the Co^{4+} ions are all in a LSS with $S = 1/2$ and located in the remaining octahedra.

Both solutions are energetically equivalent from an oversimplified ionic picture, but can be easily distinguished

TABLE II. Projection of the spin magnetic moments of Co atoms in the $\text{Sr}_6\text{Co}_5\text{O}_{15}$ ground state.

Atom	Magnetic moment
Co1	$1.0 \mu_B$
Co2	$-0.8 \mu_B$
Co3	$-0.2 \mu_B$

because solution (ii) could lead to two nonmagnetic Co atoms, whereas solution (i) will have all the atoms being magnetic. Our *ab initio* calculations confirm that the ground-state electronic structure can be well described by an ionic model with 3 Co^{4+} and 2 Co^{3+} cations [solution (ii) of our PCM]. Below, we will give further details of the electronic structure beyond this simple ionic model.

C. Electronic structure calculations

Table II shows the magnetic moments of each Co cation in the structure obtained for $U = 4.8$ eV. They are consistent with the ionic distribution that would predict two nonmagnetic $\text{Co}^{3+} : d^6$ cations to occur along the chain. Co1 is a $\text{Co}^{4+} : d^5$ cation with a magnetic moment of $1 \mu_B$. Co2 is also a $\text{Co}^{4+} : d^5$ cation and Co3 is close to a $\text{Co}^{3+} : d^6$ configuration. The details can be understood by looking at the magnetic interactions in the chain (see Fig. 2). The magnetic coupling between Co1 and Co2 is mediated by a Co3 (nonmagnetic). The overlap between Co3 and Co2 d orbitals motivates a charge transfer that explains the magnetic moments obtained for them [lowered from 1 for Co2 ($\text{Co}^{4+} : d^5$) and raised from 0 for Co3 ($\text{Co}^{3+} : d^6$)]. The Co^{4+} cations are in a LSS ($S = 1/2$), in agreement with Ref. 4. However, for our compound, both the Co^{3+} atoms are nonmagnetic (LSS) and located in octahedra.

A more realistic description of the electronic structure of the material is given by the partial density of states (DOS) plots of the various Co atoms in the structure (see Fig. 3). The material is a semiconductor, with a d - d gap of about 0.5 eV, for this particular value of U (4.8 eV). For Co1, a $\text{Co}^{4+} : d^5$ cation in a trigonal prismatic environment, we can see a fully occupied d_{z^2} level (with z the Co-chain axis), a hole in an xy -plane orbital (x^2-y^2, xy) at about 2 eV above the Fermi level, and the higher-lying d_{xz}, d_{yz} which remains unoccupied at higher energy, spin split by about 1 eV. The bands coming from Co2 ($\text{Co}^{4+} : d^5$), in an octahedral environment, present a spin splitting of about 1 eV of the e_g bands, located at 2 eV

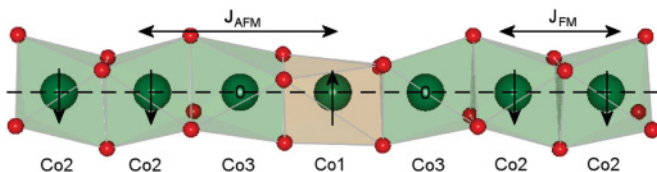


FIG. 2. (Color online) Magnetic couplings in the unit cell. We show the FM coupling between neighbor Co2 atoms and the AFM one between Co2 and Co1 mediated by a nonmagnetic Co3. The figure was obtained using VESTA (Ref. 40).

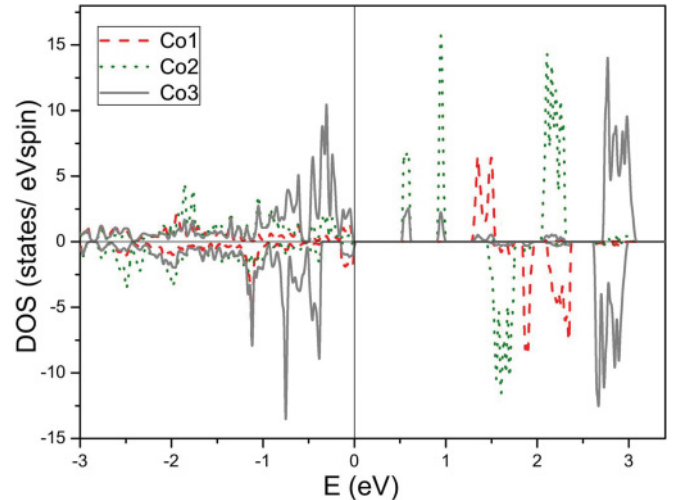


FIG. 3. (Color online) Partial spin-polarized DOS of Co1, Co2, and Co3 atoms. The Fermi energy is represented by the solid vertical line at zero. Co1 and Co2 are close to a d^5 electronic structure. Co3 is closer to a d^6 configuration with a slight unoccupied t_{2g} character.

above the Fermi level. In this case, the magnetic moment points along the minority-spin direction (the hole in the t_{2g} multiplet is in the majority-spin channel). The unoccupied t_{2g} band of Co2 presents a double-peak structure at about 1 eV above the Fermi level. We can observe an approximate d^6 DOS for Co3. Due to the hybridization between Co3 and Co2 d orbitals, a double-peak structure arises, showing a density of unoccupied t_{2g} states for Co3 much smaller than for Co2 at about 1 eV above the Fermi level, consistent with the small magnetic moment of Co3.

Two features can be observed in these plots: (i) The strongly localized nature of the electrons, with very narrow bands, less than 0.5 eV wide. The bandwidths are always smaller than the typical energies involved: both the Hund's rule coupling strength (1 eV for the e_g bands of the $\text{Co}^{4+} : d^5$ cations) and crystal-field splitting. (ii) The different crystal-field environments of the Co cations (octahedral for Co2 and Co3, trigonal prismatic for Co1) will lead to decidedly different splittings, with the e_g states of Co3 being highest in energy, at ≈ 3 eV above the Fermi level for this chosen U value of 4.8 eV. Higher U values produce a rigid shift of the bands shown in Fig. 3 with an increase of the band gap, but the description of the band structure and the main conclusions of the paper remain unchanged.

From these results, we can roughly sketch the electronic structure of $\text{Sr}_6\text{Co}_5\text{O}_{15}$: its unit cell is formed by three magnetic $\text{Co}^{4+} : d^5$ cations (one Co1 in a trigonal prismatic environment and two Co2 in an octahedral environment) and two nonmagnetic $\text{Co}^{3+} : d^6$ atoms (Co3) in an octahedral environment.

D. Magnetic properties

We have performed LDA + U calculations for several values of the on-site Coulomb repulsion term. Since we are dealing with a semiconducting d^5/d^6 system, a value of U between 4 and 8 eV is reasonable to describe it correctly.⁴¹

The magnetic ground-state solution we will describe below (magnetic moments of Co atoms in the ground state are written in Table II) is the most stable for the above-mentioned range of values of the on-site Coulomb repulsion.

Starting from the electronic structure described above, we can understand the magnetic couplings in the unit cell. Two couplings can be considered (see Fig. 2): one ferromagnetic (J_{FM}) direct exchange between nearest-neighbor magnetic Co2: d^5 cations and another one antiferromagnetic (J_{AFM}) between Co1: d^5 and Co2: d^5 mediated by a nonmagnetic cation Co3: d^6 , which acts in a similar way to O anions in the oxygen-mediated superexchange in perovskites. Both these couplings can be understood in terms of the Goodenough-Kanamori-Anderson rules.⁴² We can use our total energy calculations to describe and quantify the magnetic interactions in the unit cell (schematically depicted in Fig. 2). In order to give an estimate of the couplings along the chain, we can fit the total energies resulting from various possible collinear magnetic configurations to a Heisenberg model, in the form of $H = \frac{1}{2} \sum_{i,j} J_{ij} S_i S_j$. Calculations reveal the following values for the coupling constants $J_{FM} \approx 220$ K and $J_{AFM} \approx 6$ K (of opposite sign). As expected, the FM coupling is stronger than the AFM one that occurs between second-neighbor cations mediated by a nonmagnetic ion. Because of this peculiar magnetic arrangement, no 1D FM order (along the Co chains) is observed, but only a short-ranged FM coupling between Co2 cations survives at high temperature. The existence of an in-chain AFM coupling and two nonmagnetic Co atoms per unit cell will also affect the interchain interactions. Because the in-chain magnetic couplings are not purely FM, the magnetic properties of $Sr_6Co_5O_{15}$ can no longer be understood as FM spin chains coupled antiferromagnetically in plane, as occurs in $Ca_3Co_2O_6$.¹³ Also reasoning in terms of the hexagonal planes, the nonmagnetic planes formed by Co3 atoms which intercalate between the magnetic ones will contribute to the lowering of the interchain magnetic couplings. The total ordered moment is $1 \mu_B$ per unit cell.

Figure 4 shows the magnetic susceptibility as a function of the temperature at $H = 100$ Oe. Below 220 K a splitting between ZFC and FC curves can be observed. This effect is quite common in other cobaltates,^{43–45} and it is often attributed to spin-glass effects or other types of magnetic inhomogeneities. In our case, according to the refinement of NPD data, there is an average cobalt deficiency of about 6%. The observed effects due to magnetic inhomogeneities are brought about by an arrangement of Co^{3+} and Co^{4+} cations that are not homogeneously distributed throughout the solid. On the 5-K NPD pattern there is no additional contribution to the scattering.³⁹ Our results indicate that there is no long-range ordering over a sufficiently large coherent domain to give rise to magnetic scattering. As we have mentioned, we could be in the presence of a partially disordered structure with spin-glass-like features. In addition, the described AFM coupling found *ab initio* could perfectly take place in spatially limited regions of a structure lacking the required long-range coherence to be detected by diffraction methods.

At 32 K a kink can be noticed in the ZFC curve. This anomaly could have various origins: a blocking temperature due to magnetic inhomogeneities in the system (this maximum

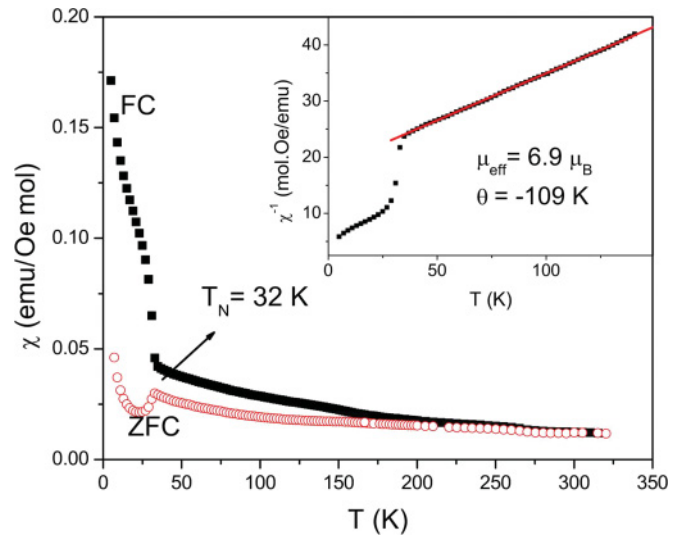


FIG. 4. (Color online) Magnetic susceptibility versus temperature measured at $H = 100$ Oe under ZFC and FC conditions. The Néel temperature that can be identified from the curves is about 32 K. The inset shows the variation of FC inverse susceptibility at low temperatures. θ represents the Curie-Weiss temperature.

would be shifted with the applied magnetic field, an effect which is not observed), it could be due to an intrinsic magnetic ordering temperature or due to Co_3O_4 inclusions, which we have identified as being $\sim 2\%$ in our sample. In order to elucidate the origin of this anomaly we have measured the magnetization versus temperature $M(T)$ curve for pure Co_3O_4 and also for a sample composed of SiO_2 with 2% of Co_3O_4 . The objective of this experiment was to determine if a very diluted Co_3O_4 sample was able to exhibit its Néel temperature using our measuring conditions. The results show that such a small quantity of Co_3O_4 is not enough to make visible the T_N in a $M(T)$ curve (see Fig. 5). Hence, the magnetic transition

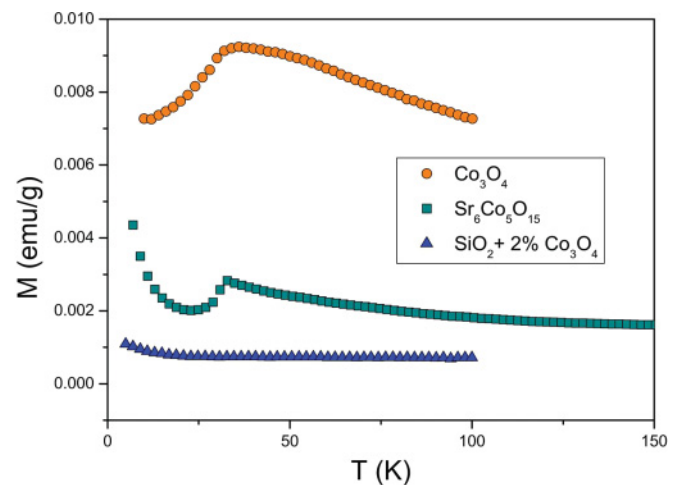


FIG. 5. (Color online) Comparison of ZFC magnetization versus temperature curve of pure Co_3O_4 , $Sr_6Co_5O_{15}$, and a solution of 2% of Co_3O_4 in SiO_2 . Observe that the cusp in the susceptibility disappears for the case of diluted Co_3O_4 , suggesting it is an intrinsic effect of $Sr_6Co_5O_{15}$.

observed in our $\text{Sr}_6\text{Co}_5\text{O}_{15}$ sample is an intrinsic effect of the compound.

The linear fitting of the $\chi(T)^{-1}$ curve in the paramagnetic region (the inset of Fig. 4) reveals a negative Curie-Weiss temperature (in agreement with that obtained by Sugiyama *et al.*⁴ for other intermediate members of the series). Based on similarities among the family of cobaltates that $\text{Sr}_6\text{Co}_5\text{O}_{15}$ structurally belongs to, and considering we do not have purely FM in-chain couplings, the kink observed at 32 K can be assigned to the existence of an interchain 2D AFM order in the triangular lattice of the *ab* plane as in the other members of the series. Because the in-chain magnetic couplings are not purely FM and a long-range FM order cannot be established along the chains, the occurrence of 1D-FM order slightly above T_N is not expected in this compound, as it occurs in other members of the series.

From our calculations, we can also obtain the value of the effective magnetic moment per formula unit and compare it with our experimental findings. Hence, taking the usual expressions for the square effective paramagnetic moment of each magnetic Co, $\mu_{\text{eff}}^2 = [g_l^2 l(l+1) + g_s^2 s(s+1)]\mu_B^2$, and considering $l = 0$ or 1 , $\mu \in [5.2, 6.7]\mu_B$ for the whole unit cell formed by five Co cations. Depending on the value of the orbital angular momentum (see below for details of our calculations), that would be the range of possible values for μ_{eff} . This is consistent with the $5.6\mu_B$ value obtained by Sun *et al.*²⁷ (if the orbital angular momenta were negligible), and it agrees with our experimental magnetic moment of $6.9\mu_B$ per formula (if the orbital angular momenta were aligned with the magnetization). This value was obtained from the linear fitting of χ^{-1} versus T curve in the paramagnetic region (see the inset of Fig. 4).

E. A peculiar quasi-one-dimensional oxide

Both end members of the series have in common an Ising-type behavior,^{13,22} with moments aligned along the chain direction with large values of magnetocrystalline anisotropy. This quasi-one-dimensionality is somehow not observed in $\text{Sr}_6\text{Co}_5\text{O}_{15}$. We have studied the system by introducing SOC in the calculations with the magnetization lying along different crystallographic directions. However, none of these directions can align the orbital and magnetic moments of all the Co atoms at the same time (see Table III). Large values of the orbital angular momenta are obtained for the Co atoms in the structure when the magnetization is set along different directions: the preferred direction for orienting their moments is different for each magnetic Co (Co1 and Co2) in the unit cell. For them, the orbital angular momentum is parallel to

TABLE III. Projection of the orbital angular momenta of Co atoms along the magnetization axis for different directions of the magnetization (in μ_B units).

	Atom l_z for various magnetization directions						
	(111)	(101)	(110)	(011)	(100)	(010)	(001)
Co1	0.99	0.75	0.66	0.72	0.41	0.36	0.44
Co2(a)	-0.05	-0.15	-0.17	-0.19	-0.22	-0.28	-0.31
Co2(b)	-0.05	-0.20	-0.18	-0.17	-0.28	-0.29	-0.27

the spin moment, as a result of Hund's third rule. For Co1, the degenerate x^2-y^2 and xy levels (where the hole resides) can form a linear combination of eigenstates with $l_z = 2$,¹³ so the $\text{Co}^{4+}:d^5$ cation in a prismatic environment is susceptible of developing a ground state with a large value of the orbital angular momentum. On the other hand, Co2 ($\text{Co}^{4+}:d^5$) can develop an $l_z = 1$ eigenstate since the t_{2g} multiplet acts as an effective $l = 1$ multiplet.⁴⁶⁻⁵⁰ The ground-state quantization axis will be related to the local environment, which is rotated for the two Co2 atoms in the unit cell. This explains why we have different l_z values even for the two equivalent Co2 atoms in the structure. Consequently, this spin system cannot be described as an Ising-type one due to the canting of the moments of the various magnetic ions with respect to each other. Such canting can be understood according to the different Co environments and as a local orientation of the moments along its particular symmetry axis. The values are summarized in Table III, and help to understand the measured μ_{eff} value.

Another difference from the other compounds in the series is that, in this case, the 2Co^{3+} atoms are nonmagnetic (LSS) and located in octahedra, while in the other members of the series one of them is in a LSS in an octahedral environment and the other one is in a HSS and located at the trigonal prismatic site. In addition, we do not have strong in-chain FM coupling for all the Co atoms in the unit cell. Thus, the magnetic properties of $\text{Sr}_6\text{Co}_5\text{O}_{15}$ cannot be understood as FM spin chains because of the AFM coupling that (though weak) occurs within them and the two nonmagnetic Co atoms in every unit cell.

Clearly, the magnetic properties of this compound differ from the other members of the series, making it less quasi-one-dimensional.

F. Transport properties

We have calculated the temperature dependence of the thermoelectric power to further analyze the system properties and the magnetic ground state. This has been done by

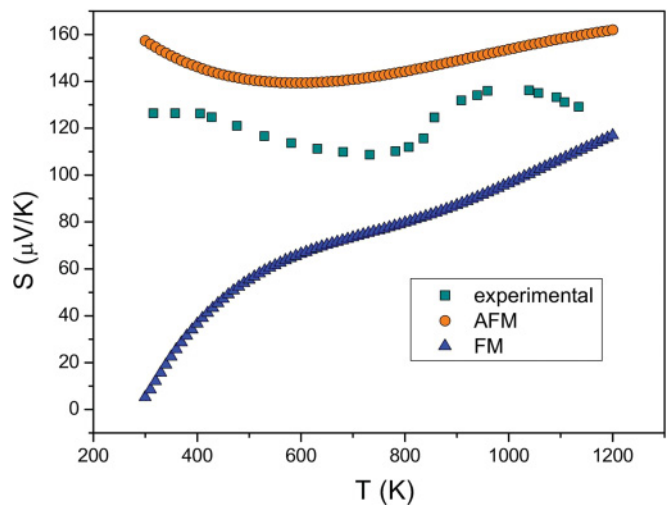


FIG. 6. (Color online) Experimental (Ref. 30) and calculated temperature dependence of the thermopower. The results for both FM and AFM spin configurations are plotted.

taking our band-structure calculations within a semiclassical approach based on the Boltzmann transport theory through the BOLTZTRAP code.³⁶ A dense grid of 10 000 k points in the full Brillouin zone has been used to obtain convergence. Taking the conductivity (σ) and Seebeck coefficient (S) calculated for both spin channels, the total thermopower has been obtained according to the two-current model expression,⁵¹

$$S = \frac{\sigma'(\uparrow)S(\uparrow) + \sigma'(\downarrow)S(\downarrow)}{\sigma'(\uparrow) + \sigma'(\downarrow)}, \quad (1)$$

where $\sigma' = \sigma/\tau$, within the constant scattering time (τ) approximation. For the sake of comparison, we present the calculations obtained for the ground-state in-chain AFM spin configuration shown in Fig. 2 and also for a FM solution (which is higher in energy according to our calculations). We present the data calculated for both spin configurations at $U = 4.8$ eV, together with the experimental values of the Seebeck coefficient taken from Ref. 30 (see Fig. 6). The results for the AFM solution fit the experimental values nicely, both in order of magnitude of the thermopower and also on the observed nonactivated evolution with the temperature. However, the FM one differs clearly from the experiment, giving further evidence of the validity of our description of the electronic structure of the compound.

IV. SUMMARY

We have synthesized $\text{Sr}_6\text{Co}_5\text{O}_{15}$, measured its magnetic properties, and performed *ab initio* calculations. The material is structurally quasi-one-dimensional and can be identified as a member of the structural series $A_{n+2}B'B_n\text{O}_{3n+3}$ of hexagonal quasi-one-dimensional Co oxides. It is a semiconducting

antiferromagnet that exhibits a magnetic transition at 32 K, showing some peculiar electronic structure properties that make it different than the other members of the series: (i) The two Co^{3+} atoms in the structure are nonmagnetic and located in octahedra. (ii) The in-chain couplings are not purely FM, and AFM couplings (though weak) occur within the chains. (iii) This, together with the existence of two nonmagnetic Co atoms in the unit cell, reduces not only the in-chain but also the interchain magnetic couplings. (iv) Due to (ii) and (iii), the magnetic properties of the material can no longer be understood as FM spin chains coupled AFM in plane as occurs in other members of the series. (v) The preferred orientation of the orbital angular momenta is noncollinear, in contrast to the strong Ising-type behavior found in $\text{Ca}_3\text{Co}_2\text{O}_6$ and BaCoO_3 . In addition, transport properties calculations support our understanding of its electronic structure and magnetic properties.

This anomalous behavior makes $\text{Sr}_6\text{Co}_5\text{O}_{15}$ less quasi-one-dimensional than expected due to its structure and helps understand the intricate structure-property relations in strongly correlated electron systems.

ACKNOWLEDGMENTS

The authors thank the CESGA (Centro de Supercomputación de Galicia) for the computing facilities and the Ministerio de Educación y Ciencia (MEC) for financial support through the project MAT2009-08165. The authors also thank the Ministerio de Ciencia e Innovación (MICINN) for the project MAT2007-60536 and the Xunta de Galicia for the project INCITE08PXIB236053PR. A.S.B. thanks MEC for a FPU grant.

*antia.sanchez@usc.es

¹K. Takada, H. Sakurai, E. Takayama-Muromachi, F. Izumi, R. A. Dilanian, and T. Sasaki, *Nature (London)* **422**, 53 (2003).

²C. Martin, A. Maignan, D. Pelloquin, N. Nguyen, and B. Raveau, *Appl. Phys. Lett.* **71**, 1421 (1997).

³M. J. R. Hoch, P. L. Kuhns, W. G. Moulton, A. P. Reyes, J. Wu, and C. Leighton, *Phys. Rev. B* **69**, 014425 (2004).

⁴J. Sugiyama, H. Nozaki, J. H. Brewer, E. J. Ansaldo, T. Takami, H. Ikuta, and U. Mizutani, *Phys. Rev. B* **72**, 064418 (2005).

⁵K. Boulahya, M. Parras, and J. M. González-Calbet, *J. Solid State Chem.* **142**, 419 (1999).

⁶K. Boulahya, M. Parras, J. M. González-Calbet, and A. Vegas, *J. Solid State Chem.* **151**, 77 (2000).

⁷K. Boulahya, M. Parras, and J. M. González-Calbet, *J. Solid State Chem.* **145**, 116 (1999).

⁸A. Maignan, C. Michel, A. C. Masset, C. Martin, and B. Raveau, *Eur. Phys. J. B* **15**, 657 (2000).

⁹H. Fjellvåg, E. Gulbrandsen, S. Aasland, A. Olsen, and B. C. Hauback, *J. Solid State Chem.* **124**, 190 (1996).

¹⁰S. Aasland, H. Fjellvåg, and B. Hauback, *Solid State Commun.* **101**, 187 (1997).

¹¹H. Kageyama, K. Yoshimura, K. Kosuge, M. Azuma, M. Takano, H. Mitamura, and T. Goto, *J. Phys. Soc. Jpn.* **66**, 3996 (1997).

¹²B. Martínez, V. Laukhin, M. Hernando, J. Fontcuberta, M. Parras, and J. M. González-Calbet, *Phys. Rev. B* **64**, 012417 (2001).

¹³H. Wu, T. Burnus, Z. Hu, C. Martin, A. Maignan, J. C. Cezar, A. Tanaka, N. B. Brookes, D. I. Khomskii, and L. H. Tjeng, *Phys. Rev. Lett.* **102**, 026404 (2009).

¹⁴J.-G. Cheng, J.-S. Zhou, and J. B. Goodenough, *Phys. Rev. B* **79**, 184414 (2009).

¹⁵H. Taguchi, Y. Takeda, F. Kanamaru, M. Shimada, and M. Koizumi, *Acta Crystallogr. Sect. B* **33**, 1298 (1977).

¹⁶K. Yamaura, H. W. Zandbergen, K. Abe, and R. J. Cava, *J. Solid State Chem.* **146**, 96 (1999).

¹⁷V. Pardo, M. Iglesias, D. Baldomir, J. Castro, and J. E. Arias, *Solid State Commun.* **128**, 101 (2003).

¹⁸V. Pardo, P. Blaha, M. Iglesias, K. Schwarz, D. Baldomir, and J. E. Arias, *Phys. Rev. B* **70**, 144422 (2004).

¹⁹V. Pardo, J. Rivas, and D. Baldomir, *Appl. Phys. Lett.* **86**, 202507 (2005).

²⁰P. M. Botta, V. Pardo, D. Baldomir, C. de la Calle, J. A. Alonso, and J. Rivas, *Phys. Rev. B* **74**, 214415 (2006).

²¹V. Pardo, P. Blaha, K. Schwarz, and D. Baldomir, *Physica B* **378**, 556 (2006).

²²V. Pardo, P. Blaha, R. Laskowski, D. Baldomir, J. Castro, K. Schwarz, and J. E. Arias, *Phys. Rev. B* **76**, 165120 (2007).

- ²³H. Nozaki, M. Janoschek, B. Roessli, J. Sugiyama, L. Keller, J. H. Brewer, E. J. Ansaldo, G. D. Morris, T. Takami, and H. Ikuta, *Phys. Rev. B* **76**, 014402 (2007).
- ²⁴J. Sugiyama, H. Nozaki, Y. Ikedo, K. Mukai, D. Andreica, A. Amato, J. H. Brewer, E. J. Ansaldo, G. D. Morris, T. Takami, and H. Ikuta, *Phys. Rev. Lett.* **96**, 197206 (2006).
- ²⁵W. T. A. Harrison, S. L. Hegwood, and A. J. Jacobson, *J. Chem. Soc. Chem. Commun.* 1953 (1995).
- ²⁶J. A. Campá, E. Gutiérrez-Puebla, M. A. Monge, I. Rasines, and C. Ruíz-Valero, *J. Solid State Chem.* **108**, 230 (1994).
- ²⁷J. Sun, G. Li, Z. Li, L. You, and J. Lin, *Inorg. Chem.* **45**, 8394 (2006).
- ²⁸M.-H. Whangbo, H.-J. Koo, K.-S. Lee, O. Gourdon, M. Evain, S. Jovic, and R. Brec, *J. Solid State Chem.* **160**, 239 (2001).
- ²⁹R. Hoffmann, *J. Chem. Phys.* **39**, 1397 (1963).
- ³⁰K. Iwasaki, M. Shimada, H. Yamane, J. Takahashi, S. Kubota, T. Nagasaki, Y. Arita, J. Yuhara, Y. Nishi, and T. Matsui, *J. Alloys Compd.* **377**, 272 (2004).
- ³¹T. Takami, M. Horibe, M. Itoh, and J. Cheng, *Phys. Rev. B* **82**, 085110 (2010).
- ³²T. Takami, H. Ikuta, and U. Mizutani, *Jpn. J. Appl. Phys.* **43**, 8208 (2004).
- ³³H. M. Rietveld, *J. Appl. Crystallogr.* **2**, 65 (1969).
- ³⁴J. Rodríguez-Carvajal, *Physica B* **192**, 55 (1993).
- ³⁵P. Blaha, K. Schwarz, G. K. H. Madsen, D. Kvasnicka, and J. Luitz, *WIEN2k, An Augmented Plane Wave Plus Local Orbitals Program for Calculating Crystal Properties* (Vienna University of Technology, Austria, 2001).
- ³⁶G. K. H. Madsen and D. J. Singh, *Comput. Phys. Commun.* **175**, 67 (2006).
- ³⁷A. I. Liechtenstein, V. I. Anisimov, and J. Zaanen, *Phys. Rev. B* **52**, R5467 (1995).
- ³⁸D. J. Singh, *Planewaves, Pseudopotentials and the LAPW Method* (Kluwer Academic, Amsterdam, 1994).
- ³⁹C. de la Calle, J. A. Alonso, and M. T. Fernández-Díaz, *Z. Naturforsch.* **63b**, 647 (2008).
- ⁴⁰K. Momma and F. Izumi, *J. Appl. Crystallogr.* **41**, 653 (2008).
- ⁴¹E. R. Ylvisaker, W. E. Pickett, and K. Koepf, *Phys. Rev. B* **79**, 035103 (2009).
- ⁴²J. B. Goodenough, *Magnetism and the Chemical Bond* (Interscience, New York, 1963).
- ⁴³D. Phelan, D. Louca, K. Kamazawa, S.-H. Lee, S. Rosenkranz, M. F. Hundley, J. F. Mitchell, Y. Motome, S. N. Ancona, and Y. Moritomo, *Phys. Rev. Lett.* **97**, 235501 (2006).
- ⁴⁴J. Wu and C. Leighton, *Phys. Rev. B* **67**, 174408 (2003).
- ⁴⁵A. Muñoz, C. de la Calle, J. A. Alonso, P. M. Botta, V. Pardo, D. Baldomir, and J. Rivas, *Phys. Rev. B* **78**, 054404 (2008).
- ⁴⁶A. Abragam and B. Bleaney, *Electron Paramagnetic Resonance of Transition Ions* (Clarendon, Oxford, 1970).
- ⁴⁷K. W. H. Stevens, *Proc. R. Soc. London Ser. A* **219**, 542 (1953).
- ⁴⁸J. B. Goodenough, *Phys. Rev.* **171**, 466 (1968).
- ⁴⁹C. Lacroix, *J. Phys. C* **13**, 5125 (1980).
- ⁵⁰W. E. Pickett and H. Eschrig, *J. Phys. Condens. Matter* **19**, 315203 (2007).
- ⁵¹H. J. Xiang and D. J. Singh, *Phys. Rev. B* **76**, 195111 (2007).